SCIENCE CHINA PRESS

SCIENCE CHINA Life Sciences
life.scichina.com link.springer.com
https://doi.org/10.1007/s11427-024-2726-8

RESEARCH PAPER

3D facial imaging: a novel approach for metabolic abnormalities risk profiling

Qianqian Peng[1†*], Yam Ki Cheung[1†], Yu Liu[1†], Yiyang Wang[1], Jingze Tan[2,3], Yajun Yang[2,3], Jiucun Wang[2,4,5], Jing-Dong J. Han[6], Li Jin[2,4,5], Fan Liu[7*] & Sijia Wang[1,8*]

[1]CAS Key Laboratory of Computational Biology, Shanghai Institute of Nutrition and Health, University of Chinese Academy of Sciences, Chinese Academy of Sciences, Shanghai 200031, China
[2]State Key Laboratory of Genetic Engineering, Collaborative Innovation Center for Genetics and Development, and Human Phenome Institute, Fudan University, Shanghai 200433, China
[3]Ministry of Education Key Laboratory of Contemporary Anthropology, Department of Anthropology and Human Genetics, School of Life Sciences, Fudan University, Shanghai 200433, China
[4]Taizhou Institute of Health Sciences, Fudan University, Taizhou, Jiangsu 225316, China
[5]Research Unit of Dissecting the Population Genetics and Developing New Technologies for Treatment and Prevention of Skin Phenotypes and Dermatological Diseases, Chinese Academy of Medical Sciences, Beijing 100730, China
[6]Peking-Tsinghua Center for Life Sciences, Academy for Advanced Interdisciplinary Studies, Center for Quantitative Biology, Peking University, Beijing 100871, China
7Department of Forensic Sciences, College of Criminal Justice, Naif Arab University of Security Sciences, Riyadh 11452, Kingdom of Saudi Arabia
[8]Center for Excellence in Animal Evolution and Genetics, Chinese Academy of Sciences, Kunming 650201, China

†Contributed equally to this work
*Corresponding authors (Qianqian Peng, email: pengqianqian@picb.ac.cn; Fan Liu, email: fliu@nauss.edu.sa; Sijia Wang, email: wangsijia@picb.ac.cn)

Received 30 June 2024; Accepted 12 September 2024; Published online 18 February 2025

The human face harbors a rich tapestry of complex phenotypic information spanning genetic, environmental, and physiological dimensions. While facial images excel in diagnosing genetic diseases, their untapped potential for predicting metabolic health presents an intriguing prospect. Metabolic Syndrome (MetS), marked by a constellation of metabolic abnormalities, poses a significant risk for various chronic diseases. Utilizing Face-Wide Association Studies (FaWAS) on a discovery cohort of 2,621 Chinese individuals and a replication cohort of 2,188 Chinese individuals, we investigated the associations between facial features and MetS and its related conditions. Our findings highlight half of our investigated facial features strongly correlated with MetS risk, such as a slender forehead, a broader and shorter jawline, and fuller features around the temples-eye-cheek region, with notable genetic correlations (0.55–0.58) and influences from environmental factors like age, urban residency, and educational level. The developed face-based prediction model demonstrated significant predictive robustness, achieving an AUC of up to 0.87 for MetS and 0.89 for obesity in external validations, surpassing traditional 2D imaging techniques. Our model also aids in identifying subtypes within healthy populations, with a 2.07 to 2.40-fold increased risk of developing different metabolic disorders within the next five years. This paves the way for precise risk stratification of individuals who are 'at risk'. Integrating 3D facial imaging for metabolic health predictions, our research introduces an innovative, non-invasive framework for health assessment and subtype identification, demonstrating high potential in personalized medicine and health monitoring.

3D face | metabolic syndrome | metabolic abnormalities | risk profiling | prediction | health monitoring

INTRODUCTION

The human face, a rich source of high-dimensional phenotypes, encapsulates genetic, environmental, and physiological information, providing a unique window into an individual's health status (Bonfante et al., 2021; Cui and Leclercq, 2017; Gurovich et al., 2019; Liu and Feng, 2023; Liu et al., 2023; White et al., 2021; Xiong et al., 2019; Xiong et al., 2022; Zhang et al., 2022). Mapping facial features to health status shows promise in the realm of non-invasive health monitoring with great potential in revolutionizing how we manage and understand health risks. Recent advances in 3D imaging technology have significantly enhanced the potential of facial studies, especially in medical/genetic research. Compared with 2D portraits, the extra dimension significantly enhances the phenotypic variance detectable by facial images, allowing for detailed phenotype analysis (Yang et al., 2022).

Historically, facial imaging has played a pivotal role in the diagnosis of genetic anomalies, such as Down syndrome and de Lange syndrome (Bhuiyan et al., 2006; Cox-Brinkman et al., 2007; Gurovich et al., 2019; Hammond, 2007; Hammond et al., 2008; Hammond et al., 2005; Hammond et al., 2004; Tobin et al., 2008), underscoring its diagnostic value. However, its utility in forecasting the onset of common and polygenic conditions/disorders like metabolic syndrome (MetS) remains underexplored. MetS is a multifaceted condition characterized by a cluster of metabolic abnormalities, including obesity, hyperglycemia, hypertension, and dyslipidemia (Grundy et al., 2005). The global prevalence of MetS is currently estimated to be between 25% and 35% (Saklayen, 2018). In Chinese residents aged 20 years or

Citation: Peng, Q., Cheung, Y.K., Liu, Y., Wang, Y., Tan, J., Yang, Y., Wang, J., Han, J.D., Jin, L., Liu, F., et al. 3D facial imaging: a novel approach for metabolic abnormalities risk profiling. Sci China Life Sci, https://doi.org/10.1007/s11427-024-2726-8

older, the standardized prevalence of MetS was reported to be 31.1% in 2015–2017 (Zhao et al., 2023). MetS serves as a precursor to various chronic diseases and contributes to all-cause mortality (Agirbasli and Aksoy, 2019; Cai et al., 2019; Doosti-Irani et al., 2019; Gunn et al., 2015; Hong et al., 2017; Khunti et al., 2018; Kim et al., 2018; Kontopantelis et al., 2015; Rutter and Nesto, 2011; Tsigos et al., 2013) and acts as a harbinger for various chronic ailments, thereby epitomizing a complex phenotype ideal for assessing the efficacy of facial analysis in health status determination. The identification of facial variations linked to early risk indicators of such conditions could pave the way for the development of swift, non-invasive monitoring techniques, thereby broadening the spectrum and accessibility of medical assessments.

In this context, we delve into the utility of 3D facial imaging as a non-intrusive methodology for profiling the risk of MetS by initiating a Face-Wide Association Study (FaWAS) encompassing 2,621 individuals of Chinese Han descent. This study is complemented by a subsequent prediction analysis in 2,188 Chinese individuals to evaluate the accuracy of health status prediction derived from face reading. Notably, our investigation went beyond simply predicting health status. We explored the underlying mechanisms by revealing a genetic basis for the association between facial features and health. Furthermore, we established the clinical significance of facial feature-based prediction by defining health subtypes and validating their potential in identifying high-risk populations for MetS using a longitudinal data.

Table 1. Description of samples and traits utilized in this study

Characteristic	TZL		NSPT	
	N | mean	% | sd	N | mean	% | sd
N	2,621	100.0	2,188	100.0
Male	786	30.0	778	35.6
Age (year)	55.3	9.3	49.8	13.6
MetS	840	32.1	610	28.3
Obesity	321	12.2	306	14.0
Central Obesity	810	30.9	945	43.2
Hypertension	1,184	45.2	755	34.5
Dyslipidemia	846	32.3	794	36.3
Hyperglycemia	341	13.0	182	8.3
Waist circumference (cm)	81.7	9.4	82.1	10.2
BMI (kg m^{-2})	24.4	3.2	24.2	3.6
SBP (mmHg)	134.1	19.8	127.8	20.5
DBP (mmHg)	79.9	12.3	79.6	12.0
CH (mmol L^{-1})	5.3	1.0	5.1	1.1
TG (mmol L^{-1})	1.6	1.1	1.3	0.9
HDL (mmol L^{-1})	1.6	0.4	1.4	0.4
LDL (mmol L^{-1})	3.0	0.6	3.0	1.0
GLU (mmol L^{-1})	6.0	1.4	5.6	1.0
Urban	2,150	82.0	481	22.0
Ever Smoking	548	20.9	500	22.9
Ever Alcohol consumer	458	17.5	367	16.8

RESULTS

Sample characteristics

Two cross-sectional datasets and one longitudinal dataset were included in this study: the discovery dataset, a subset of Taizhou longitudinal cohort (Wang et al., 2009) (TZL, n=2,621, 30.0% male, mean age 55.33 years±9.3 years), and the validation dataset, a subset of the National Survey of Physical Traits (Peng et al., 2024) (NSPT, n=2,188, 35.6% male, mean age 49.77 years ±13.6 years) (Figure 1A, Table 1). We also incorporated data from a longitudinal cohort study, Jidong Cohort (Xia et al., 2020) (JD), to further validate our findings and assess the long-term predictive potential of facial feature-based health subtypes. This dataset includes follow-up data of 3,769 individuals collected over five years across four time points: 2018, 2019, 2022, and 2023.

In our study, an individual was classified as having MetS according to the revised ATP III (Third Adult Treatment Panel Report) criteria (Huang et al., 2022). The definition of other diseases (Obesity, Dyslipidemia, Hypertension, Hyperglycemia, etc.) could be found in Methods. The prevalences of these metabolic conditions, including metabolic syndrome (28.3%–32.1%) and hypertension (34.5%–45.2%), were largely consistent with previously reported epidemiological data in Chinese populations (Chen et al., 2023; Ge et al., 2020; Li et al., 2020; Lu et al., 2021; Mu et al., 2021; Yin et al., 2022).

Our 3D imagery analysis ascertained 7,906 spatially dense facial landmarks, resulting in a total of 23,718 vectors on the x-y-, and z- dimensions. The top 100 principal components (PCs) underlying these facial vectors could explain 94% of the total facial variance, while the top 50 PCs explained 89% (Figure 2A and B, Table S1). Many PCs also demonstrated highly significant associations with age and sex as expected (P-value < 0.05) (Table S1).

Abundant face associations with health status

Our FaWAS examined the association between the 23,718 facial vectors and the risk of MetS (Figure 1A), revealing that nearly half of the facial vectors (47.6%, n=11,296) showed a significant association with MetS risk even after a conservative Bonferroni adjustment (P-value$\leqslant 2.1\times10^{-6}$, Figure 1B). The strongest association was observed in the cheek region, marked by the most significant P-value of 5.6×10^{-68}. Visual analysis of these associations corroborated our observations that individuals with MetS commonly exhibit a narrower forehead, a wider and shorter jawline, and fuller features around the temples, eyes, and cheeks (Figure 1C, Figure S3C).

A replication study in a second population (NSPT) confirmed these associations with a high replication rate. Notably, among the 11,296 significant facial vectors identified in the discovery data (TZL), a substantial proportion (76.8%, n=8,676) remained significant even after a strict Bonferroni correction (P-value$<4.4\times10^{-6}$) (Figure S1A, Table S2). Importantly, these associations were consistent across genders, as evident by the strong correlations in effect sizes between males and females (Pearsons' r = 0.9 in TZL and r = 0.87 in NSPT, Figure S2A and B).

Further analysis involving additional 14 MetS-related disorders and traits revealed similar association patterns. A considerable number of facial vectors were significantly associated with MetS-related metabolic abnormalities (ranging from

https://doi.org/10.1007/s11427-024-2726-8

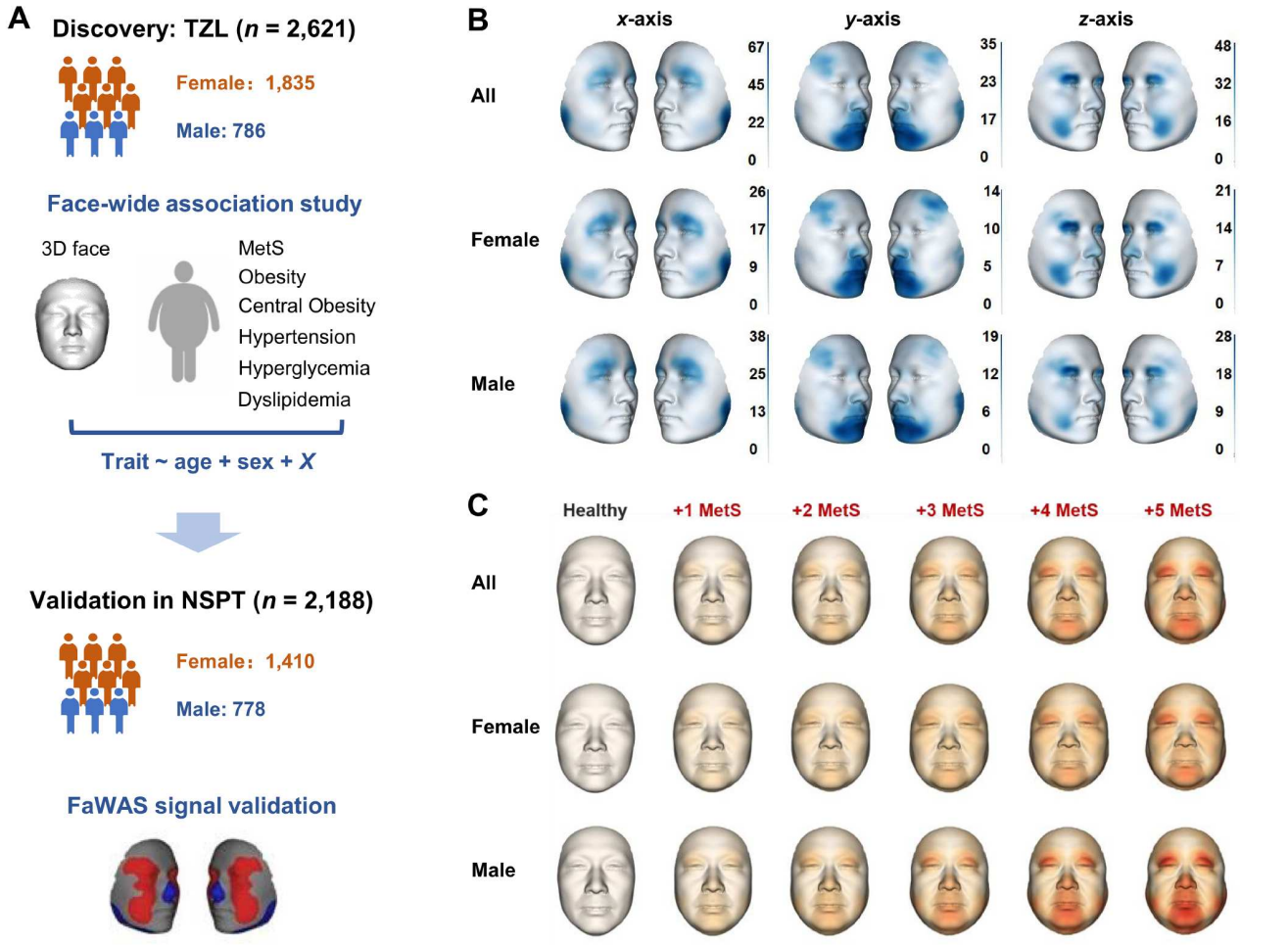

Figure 1. FaWAS result of Metabolic syndrome (MetS). A, FaWAS design in this study. B, –log10 transformed *P* values of FaWAS result of MetS in the discovery cohort. Gradient blue indicates –log10 transformed *P* values of FaWAS result of MetS. C, The average facial appearance of healthy individuals and individuals with MetS. +1 MetS indicates the average face of individuals with MetS; +2 to +5 indicates 2 to 5 times amplified metabolic syndrome facial effects.

13.3% for hyperglycemia up to 50.0% for obesity) and traits (from 16.9% for GLU up to 65.5% for BMI, Table S2, Figure S1B–S1H). Notably, the most associated facial regions for BMI (wider and shorter jaw) closely aligned with findings in previous studies using 2D facial imaging (Figure S4) (Stephen et al., 2017; Wen and Guo, 2013). The diagnostic criteria for metabolic syndrome include waist circumference, blood pressure (SBP and DBP), blood glucose, and blood lipids (HDL, TG). Increased waist circumference and TG were associated with a narrower and shorter forehead, a wider and shorter mandible, and fuller features around the temples, eyes, and cheeks. Increased waist circumference was also associated with a sunken nasal area (Fig. S5A and B). These features are consistent with the characteristics of facial obesity. Elevated SBP and DBP were associated with a narrower and fuller forehead, as well as a shorter mandible (Fig. S6A–D). Elevated HDL was associated with a wider and longer forehead, a longer mandible, and sunken areas around the eyes and cheeks. This is consistent with the function of HDL, which can remove excess cholesterol from peripheral tissues and transport it back to the liver, where it is then excreted in the bile (Fig. S7A and B).

High replication rates were also observed in NSPT (ranging from 20% to 50%), with consistent findings between genders ($0.66<r<0.98$) for MetS-related disorders and traits (Table S2, Figure S1B–H and Figure S2C–P). These results highlight the profound degree to which facial characteristics are associated with health conditions, exceeding our preliminary expectations and prompting our further analysis into prediction modeling.

Facial PCs associated with MetS

In our FaWAS using facial PCs over facial vectors, we incorporated age and sex as covariates to adjust for their potential confounding effects. Despite these adjustments, the analysis consistently revealed a significant association between facial PCs and the risk of MetS, as well as its related metabolic abnormalities (Table S1). Out of the top 100 PCs, 24 were significantly associated with MetS risk, with notable associations also found with risk of obesity (22 PCs), central obesity (25 PCs), dyslipidemia (14 PCs), hyperglycemia (14 PCs), and hypertension (12 PCs). PCs that are significantly associated with MetS are also moderately to strongly associated with other metabolic diseases (Figure 2C, Table S1). For example, PC2 and PC3 are the two PCs most significantly associated with MetS (PC2: *P*-value $=1.6\times10^{-33}$, PC3: *P*-value $= 1.1\times10^{-76}$), and they are also significantly associated with five other metabolic

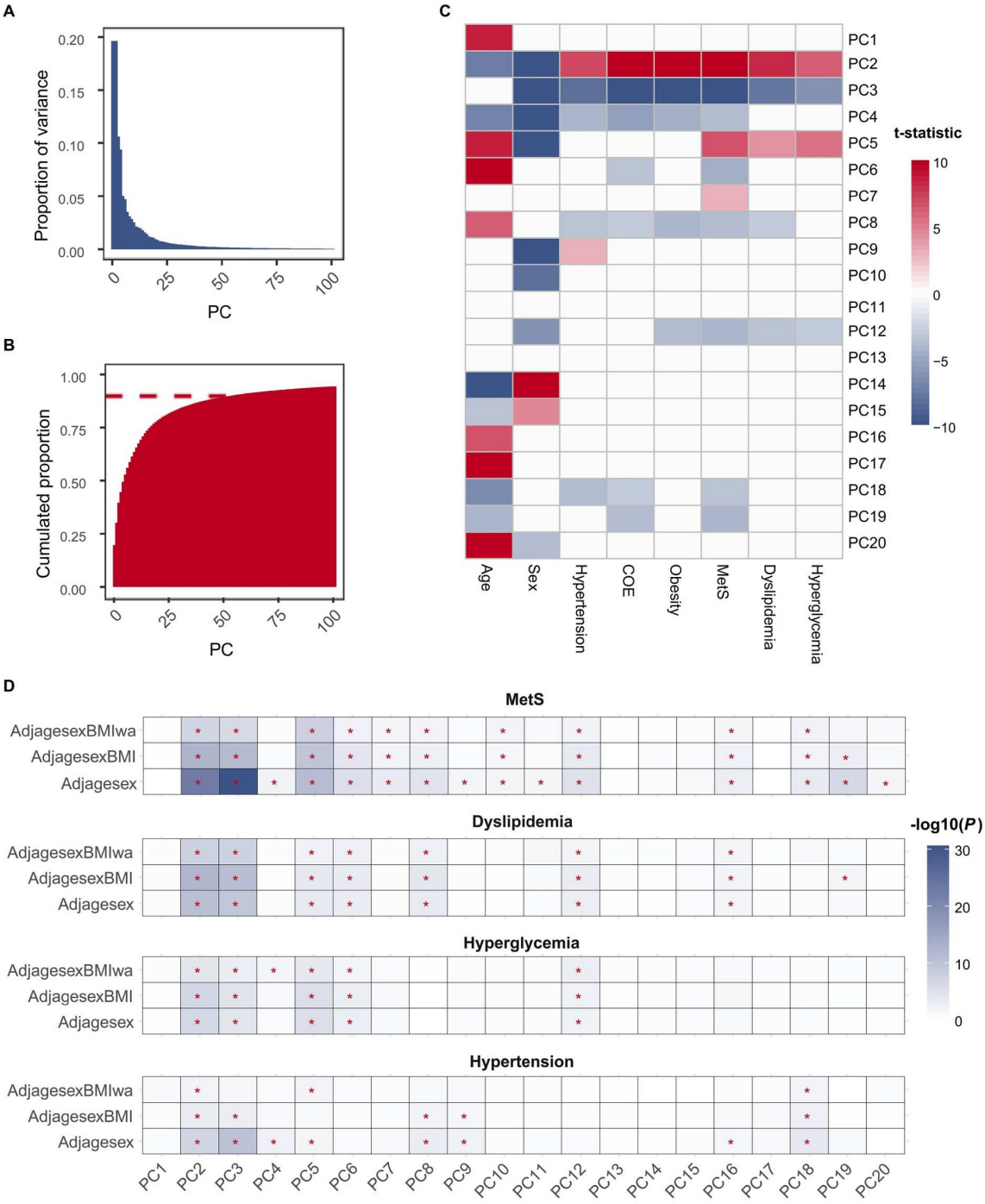

Figure 2. Facial PCs and their association with age, sex and six metabolic abnormalities. A, The explained proportion of each facial PC. Top 100 PCs were shown. B, The cumulated proportion of top 100 facial PCs. C, The association between top 20 PCs with age, sex and six metabolic abnormalities. D, The association between top 20 PCs with metabolic abnormalities age adjusted for age+sex (adjagesex), age+sex+BMI (adjagesexBMI), and age+sex+BMI+waist circumference (adjagesexBMIwa). *, significant after Bonferroni correction (P-value<2.5×10^{-4}).

disorders. Interestingly, the association of PC2 with six metabolic disorders is opposite to their association with age, and the association of PC3 with age is not significant (Figure 2C, Table S1), indicating that although metabolic disorders are age-related diseases, their manifestations on the human face are not completely synchronized with age. Obesity is a known risk factor for multiple metabolic diseases. To assess whether the observed associations between facial PCs and metabolic diseases are solely driven by obesity, we explored the relationships after controlling for obesity-related measures (BMI and waist circumference). Results revealed that even after adjusting for these obesity measures, a substantial number of facial PCs remained significantly associated with metabolic diseases (Figure 2D). This suggests that facial PCs may reflect broader metabolic dysregulation beyond that directly attributable to obesity.

https://doi.org/10.1007/s11427-024-2726-8

Common factors influencing facial variation and metabolic abnormalities

To further understand the associations between facial features and risk of metabolic abnormalities, we initiated a preliminary exploration of potential common factors influencing both facial variations and MetS risk. By leveraging data from genetic association studies related to facial morphology (Zhang et al., 2022), we aimed to quantify the genetic correlation between facial PC attributes and MetS. GCTA (Yang et al., 2011; Yang et al., 2016) was employed to estimate SNP-based heritability for facial PCs and MetS and to evaluate genetic correlations between facial PCs and MetS. Our findings reveal that although the heritability of MetS aligns with prior research (Musani et al., 2017; Rana et al., 2022), indicating a moderate range (0.22–0.24), the genetic correlation between facial features and MetS is considerably higher, marked at 0.55–0.58 (Figure 3A). This significant correlation suggests a robust shared genetic foundation underpinning both facial characteristics and MetS susceptibility.

Demographic and lifestyle factors exert significant influences on both health outcomes and physical characteristics (Gunn et al., 2015; Peng et al., 2023; Rippe, 2018; Santos, 2022). In this investigation, we analyzed eight such factors across two cohorts, aiming to pinpoint influences that concurrently affect facial characteristics and health status. Our analyses underscore the profound impact of age, urban residency, and educational attainment on both facial features and the risk of Metabolic Syndrome (MetS) (Figure 3B, Table S3). Additionally, age and educational level were also associated with central obesity, hypertension, and other metabolic conditions (Figure S8A and B, Table S4). Notably, individuals with higher levels of education displayed a reduced risk of MetS and associated metabolic diseases, alongside distinctive changes in facial features. Similarly, urban residents exhibited an increased risk of MetS compared to their rural counterparts, with corresponding significant alterations in their facial characteristics.

3D facial images accurately predict metabolic abnormalities

We investigated the potential of facial features as predictors for MetS by constructing a multiple logistic regression model that incorporates significant facial PCs from the TZL cohort (Figure 4A). Through a 10-fold cross-validation process, this model showcased a reasonable level of accuracy in predicting MetS, achieving an AUC of 0.78. When we applied this TZL-derived prediction model to NSPT, serving as an external validation set, it maintained a consistent AUC of 0.78 (Figure 4B), indicating its robust predictive capability across different populations.

To explore the viability of leveraging 3D facial variables for forecasting a broader spectrum of metabolic abnormalities, we developed predictive models for six metabolic conditions (obesity, central obesity, hypertension, dyslipidemia, hyperglycemia, and triglycerides). These models exhibited commendable efficacy in predicting the discussed disorders and traits. Notably, the model for obesity displayed an AUC of 0.79 during a 10-fold cross-validation and achieved an AUC of 0.86 within an external validation cohort (Figure 4C). Similarly, the model for central obesity registered an AUC of 0.79 during cross-validation and 0.83 in external validation (Figure 4D). The models for hypertension, dyslipidemia, and hyperglycemia also demonstrated moderate predictive performance (AUC range from 0.69 to 0.76, Figure 4E–G, Table S5), underscoring the potential of 3D facial analysis in identifying a range of metabolic disorders and traits.

Given the wealth of large-scale GWAS studies on metabolic disorders and their markers, we investigated if including genetic information could enhance the prediction accuracy of these disorders. We downloaded comprehensive GWAS summary

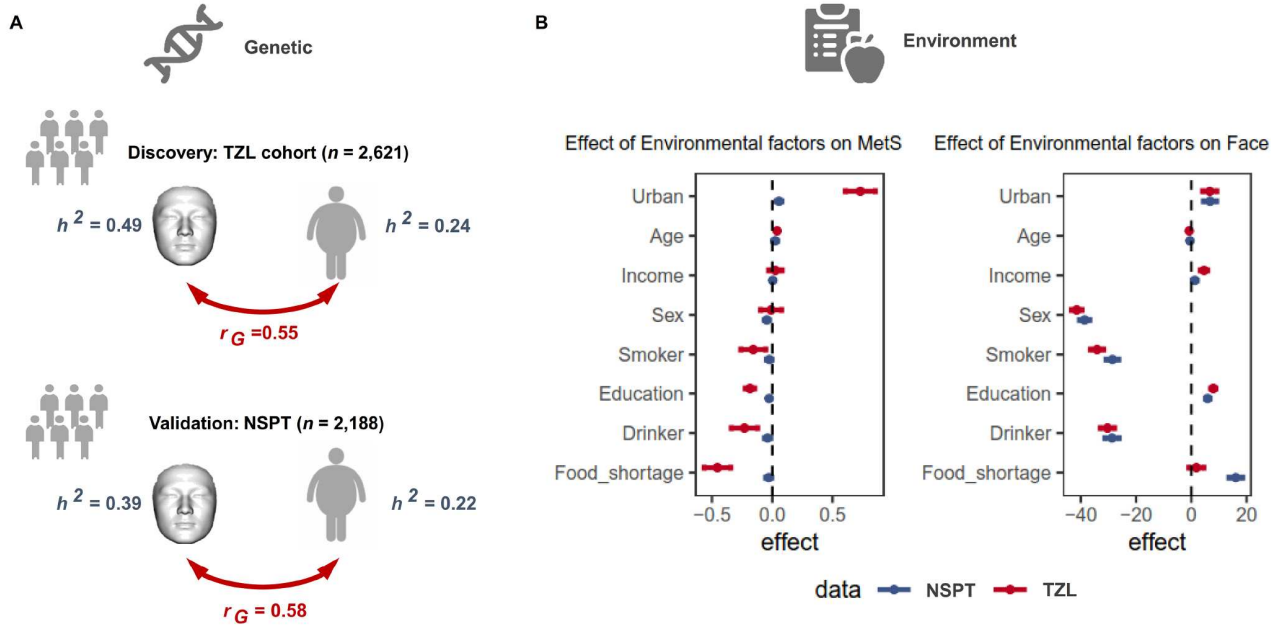

Figure 3. Genetic and environment influence both facial features and Metabolic Syndrome. A, Genetic correlation between face and MetS in TZL and NSPT. B, The effect of lifestyles on face and MetS in TZL and NSPT.

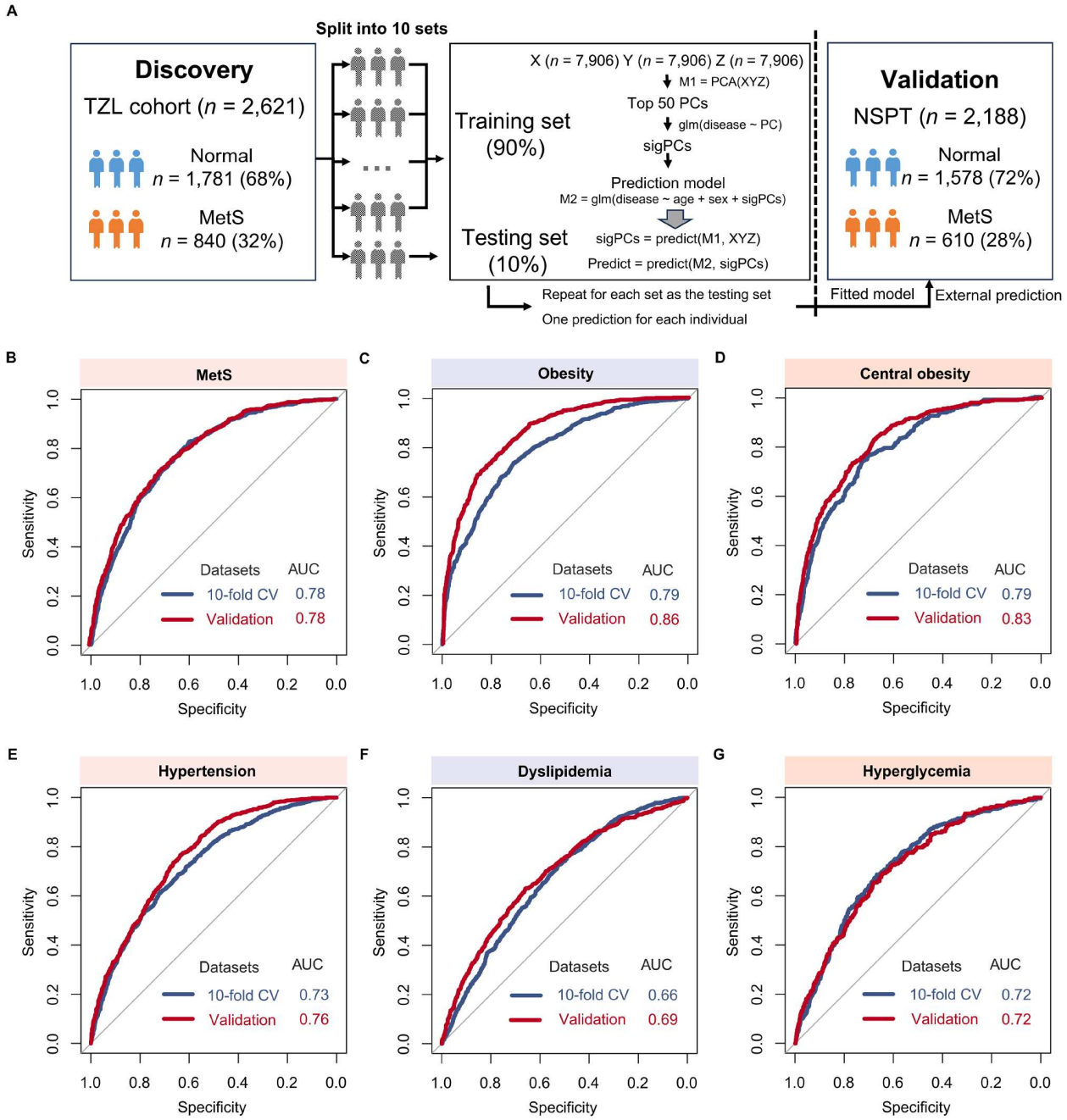

Figure 4. prediction of MetS and related metabolic abnormalities. A, Overview of study cohorts and face-based model generation. B–G, ROC curve depicting the performance of face-based models for MetS (B), Obesity (C), Central Obesity (D), Hypertension (E), Dyslipidemia (F) and Hyperglycemia (G).

statistics from various populations encompassing metabolic disorder indicators. Leveraging this data, we calculated Polygenic Risk Scores (PRS) for the relevant disorders and indicators. Subsequently, we built a model that combined facial features and PRS to predict metabolic disorders. However, this combined model did not demonstrate a significant advantage over the model relying solely on facial features (Figure S9G–L). Therefore, for subsequent analyses, we opted to utilize the prediction results based on facial features.

In gender-specific analyses, prediction models demonstrated slight, nonsystematic differences between genders across conditions, with AUCs ranging narrowly—MetS (0.75–0.78), central obesity (0.73–0.84), and obesity (0.79–0.87) in both cross-validation and external validation phases (Figure S10A–C).

Multitasking for joint disease prediction

Given that metabolic diseases often co-occur in individuals, we investigated the effectiveness of a multitask learning approach for simultaneously predicting multiple diseases (Fig. 5A). We trained two types of multitask models: random forest and multivariate regression. While the multitask model's premise aligns well with the interconnected nature of these diseases, its performance did not show a statistically significant improvement compared to

https://doi.org/10.1007/s11427-024-2726-8

single-disease models. Interestingly, both multitask models (Fig. 5B and C, 5E and F) yielded slightly lower performance compared to models trained on individual diseases (Fig. 5D and G). For instance, the multitask approaches achieved AUCs of 0.71 (Fig. 5B) and 0.72 (Fig. 5C) for MetS prediction on the external NSPT dataset, compared to the single-task model's AUC of 0.87 (Fig. 5D). Similarly, for obesity prediction, the multitask models yielded AUCs of 0.70 (Fig. 5B) and 0.79 (Fig. 5C), while the single-task model achieved an AUC of 0.89 (Fig. 5D). This trend is also reflected in other evaluation metrics like recall and F1-score, suggesting that neither multitask approach yielded statistically significant improvements over the single-task model's predictions (Fig. 5E–G). We hypothesize that this might be due to our relatively small sample size, potentially limiting the model's capacity to learn the complex relationships between facial features and multiple diseases simultaneously. This limitation could likely be addressed by expanding the sample size in future studies.

Linking facially inferred and traditional metabolic measures

Metabolic abnormalities are identified through specific anthropometric and clinical metrics, such as waist circumference, blood pressure, glucose levels, and lipid profiles. Our study explored the connection between facially inferred metabolic abnormalities and these conventional measures. Notably, classical MetS correlated significantly with seven out of nine evaluated measures after Bonferroni correction (P-value$\leqslant 9.3\times10^{-4}$) (Figure 6B). Although there were minor differences in effect sizes, these MetS-related measures consistently aligned with facially inferred MetS (Figure 6B, Table S6). Similarly, the relationship between facially inferred metabolic abnormalities and clinical markers for other metabolic conditions mirrored the associations seen with traditionally defined diseases (Figure 7B, Figure S11, Table S6). This indicates that facially inferred metabolic abnormalities closely reflect the characteristics of their traditionally identified

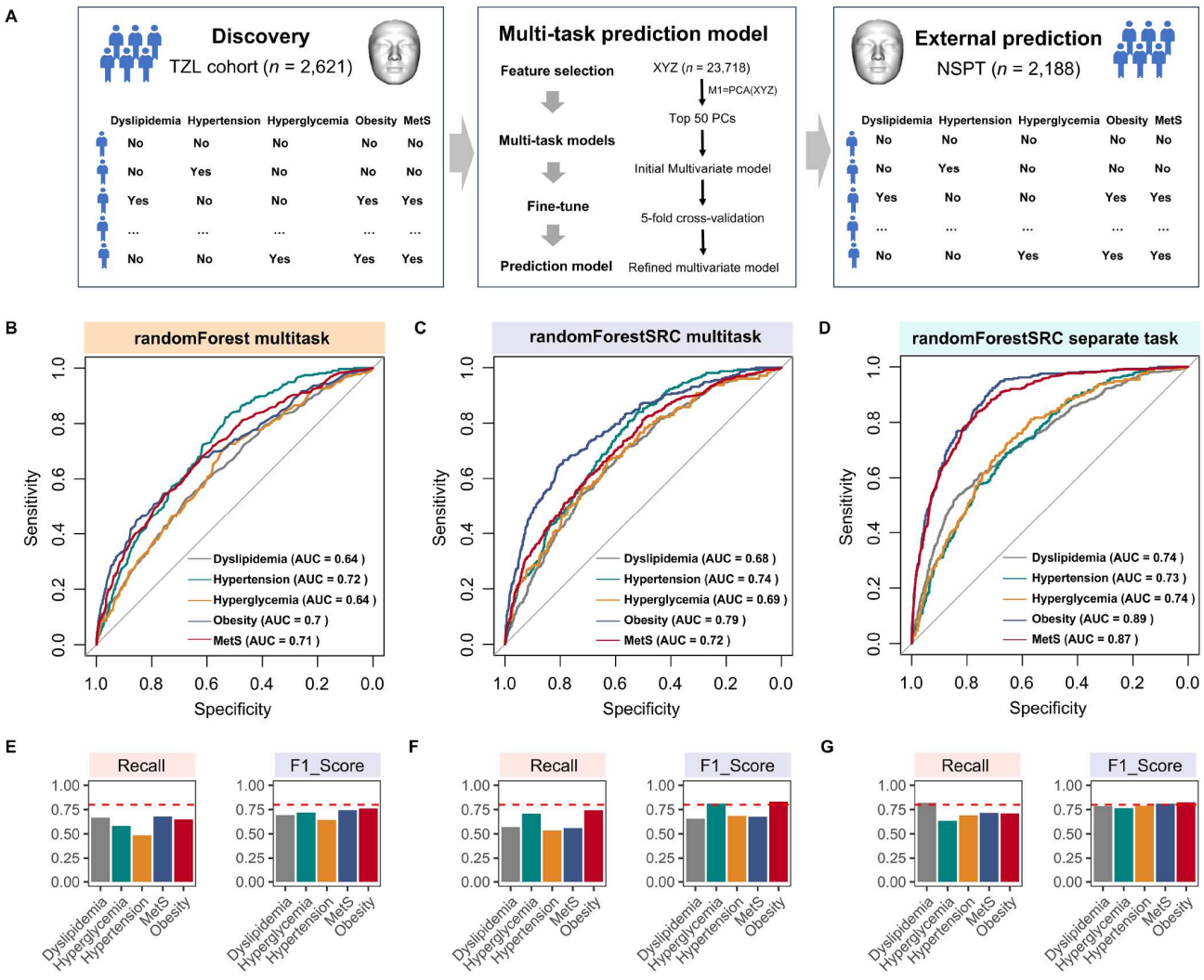

Figure 5. Performance of Multitasking for Joint Disease Prediction. A, Overview of multitask-based prediction for multiple metabolic diseases. B, Area under the curve (AUC) for predicting metabolic diseases in the external validation set (NSPT) using the Random Forest multitask prediction model; C, AUC for predicting metabolic diseases in the external validation set (NSPT) using the Random ForestSRC multitask prediction model; D, AUC for predicting metabolic diseases in the external validation set (NSPT) using the Random ForestSRC single-task prediction model; E, Recall and F1-score for predicting metabolic diseases in the external validation set (NSPT) using the Random Forest multitask prediction model; F, Recall and F1-score for predicting metabolic diseases in the external validation set (NSPT) using the Random ForestSRC multitask prediction model; G, Recall and F1-score for predicting metabolic diseases in the external validation set (NSPT) using the Random ForestSRC single-task prediction model.

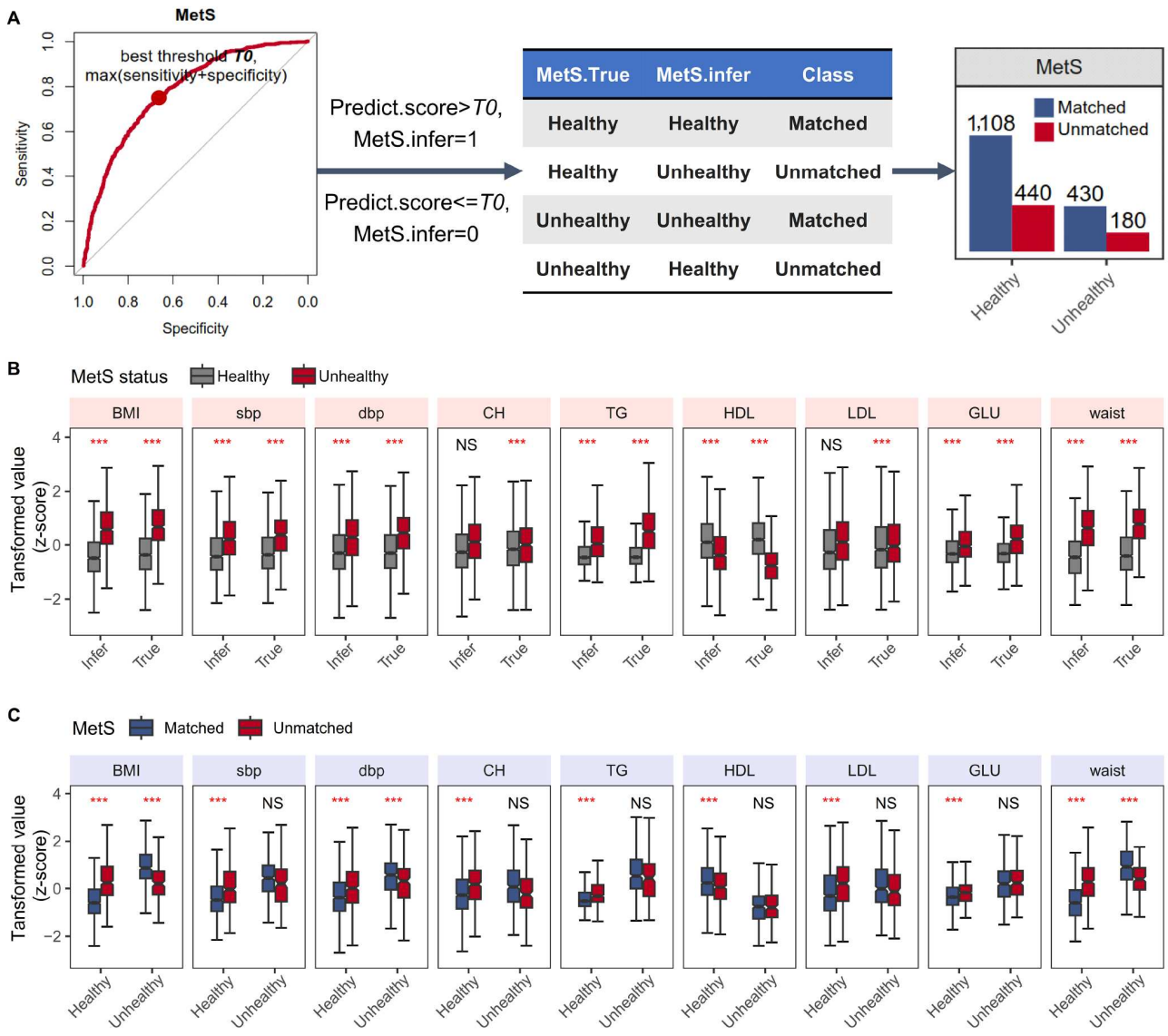

Figure 6. Misclassification of normal and MetS according to face-inferred MetS. A, The definition of matched and unmatched subgroups in normal and MetS categories according to face-inferred MetS. B, The difference of metabolic indicators between heathy and unhealthy groups defined by traditional MetS definition or face-inferred MetS status. C, The difference of metabolic indicators between matched and unmatched subgroups in traditional defined healthy and unhealthy individuals. NS, not significant (P-value$\geqslant 8.93\times10^{-4}$; ***, significant after Bonferroni correction (P-value$<8.93\times10^{-4}$)

counterparts in relation to anthropometric and clinical indicators.

Bridging facial inferred metabolic health and clinical classifications

Facially inferred MetS closely matched the phenotypic profiles of traditional MetS diagnoses, yet we observed notable variances, particularly in the associations of low-density lipoprotein (LDL) and cholesterol (CH) with traditional MetS (LDL, P-value=0.002; CH, P-value=0.004) compared to their stronger correlations with facially inferred MetS (LDL, P-value=9.3×10^{-14}; CH, P-value=8.3×10^{-18}, Figure 6B, Table S6). This discrepancy prompted an investigation into the predictive capabilities of facially inferred MetS for classifying metabolic health. In the NSPT cohort, we integrated facial predictions with clinical diagnoses to classify individuals into four groups: concordant healthy (n=1,108), concordant unhealthy (n=430), discordant healthy (n=440), and discordant unhealthy (n=180). Regardless of their clinical diagnosis, individuals in discordant groups showed physiological and biochemical markers more aligned with their facially inferred status (Figure 6C, Table S7). Specifically, clinically healthy individuals identified as having MetS through facial features exhibited markers characteristic of MetS, while clinically diagnosed MetS individuals predicted to be healthy showed healthier markers, like lower BMI and blood pressure. These findings highlight the utility of facial predictions in detecting at-risk individuals within a healthy population and refining the classification within the MetS-diagnosed group.

Further analyses applying this approach to other metabolic diseases, including hypertension, hyperglycemia, dyslipidemia, obesity, and central obesity, yielded consistent results (Figure 7B,

https://doi.org/10.1007/s11427-024-2726-8

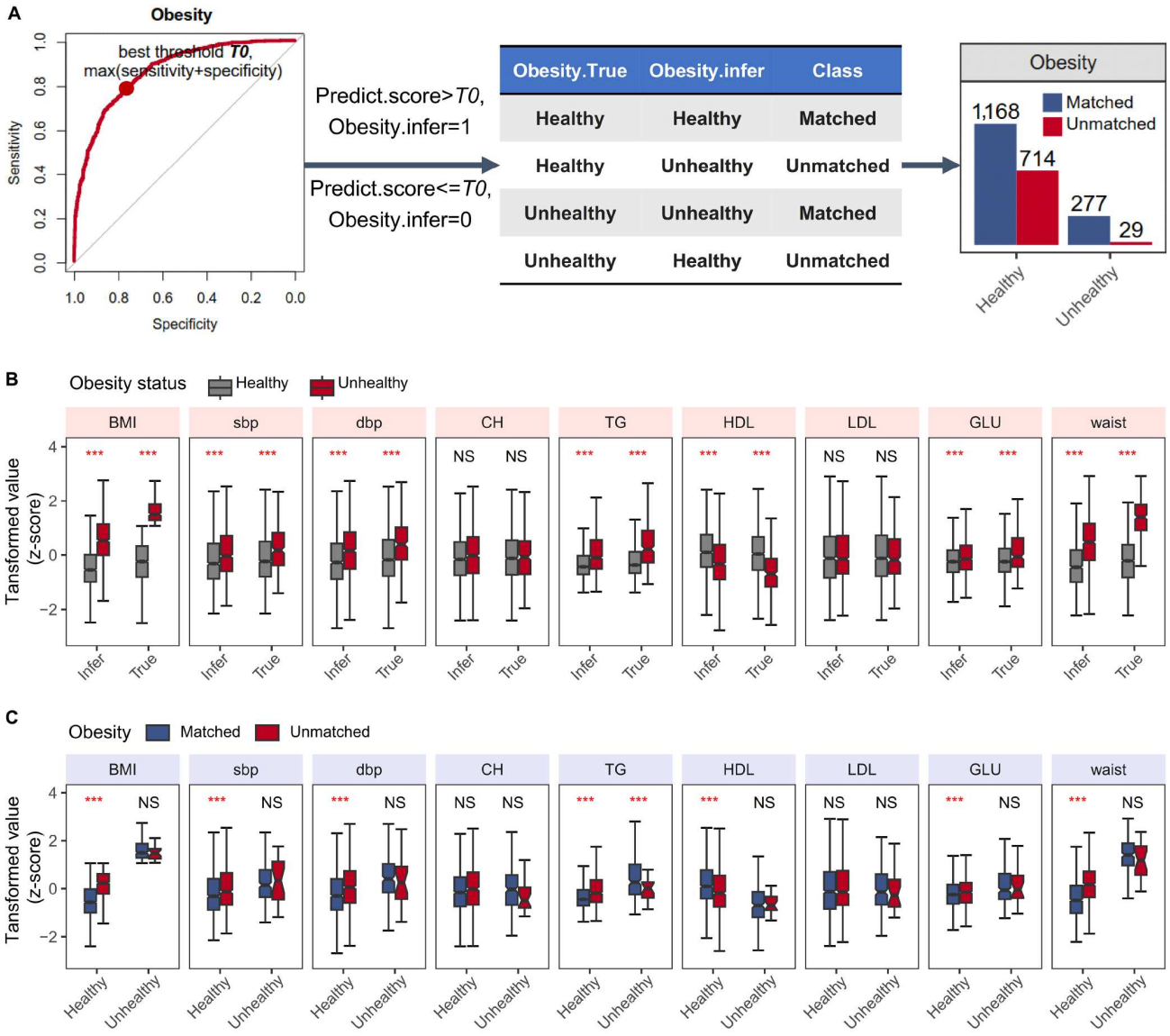

Figure 7. Misclassification of normal and obesity according to face-inferred obesity. A, The definition of matched and unmatched subgroups in normal and obese groups according to face-inferred MetS. B, The difference of metabolic indicators between heathy and unhealthy groups defined by traditional obesity definition or face-inferred obesity status. C, The difference of metabolic indicators between matched and unmatched subgroups in traditional defined healthy and unhealthy individuals. NS, not significant (P-value$\geqslant 8.93\times10^{-4}$; ***, significant after Bonferroni correction (P-value$<8.93\times10^{-4}$)

Figure S12). A previous study utilized a multi-omics approach to predict obesity found that multi-omics predictions could aid in identifying obesity subtypes (Watanabe et al., 2023). Our study revealed that face-based obesity predictions also demonstrated that individuals in the unmatched groups displayed physiological and biochemical markers that resembled the opposite category (Figure 7C, Table S8). This suggests that face-inferred disease status holds promise as a generalizable tool for uncovering subtypes within both healthy and diseased populations.

Longitudinal data validation of future disease risk in healthy subtype

Facial analysis shows promise in identifying individuals within a healthy population who may be at higher risk of developing metabolic diseases. To validate whether these predicted subgroups differ in disease susceptibility, we analyzed data from a longitudinal cohort (JD)(Xia et al., 2020). This cohort included 3,769 individuals who had 3D facial scans taken at baseline (year 2018). Additionally, the cohort has clinical information related to four metabolic diseases (obesity, hypertension, hyperglycemia, and dyslipidemia) collected in 2018 (baseline), 2019, 2022, and 2023 (Figure 8A). Although we couldn't diagnose metabolic syndrome due to missing waist circumference data, we used information on four related diseases to assess if the predicted subgroups differed in their future risk of developing them.

We applied the prediction models developed using the discovery set TZL to the JD baseline data to obtain predicted labels for the four diseases (Figure 8B). The area under the curve (AUC) for these predictions ranged from 0.68 for hypertension to 0.8 for obesity (Figure 8C). Based on the true and predicted labels,

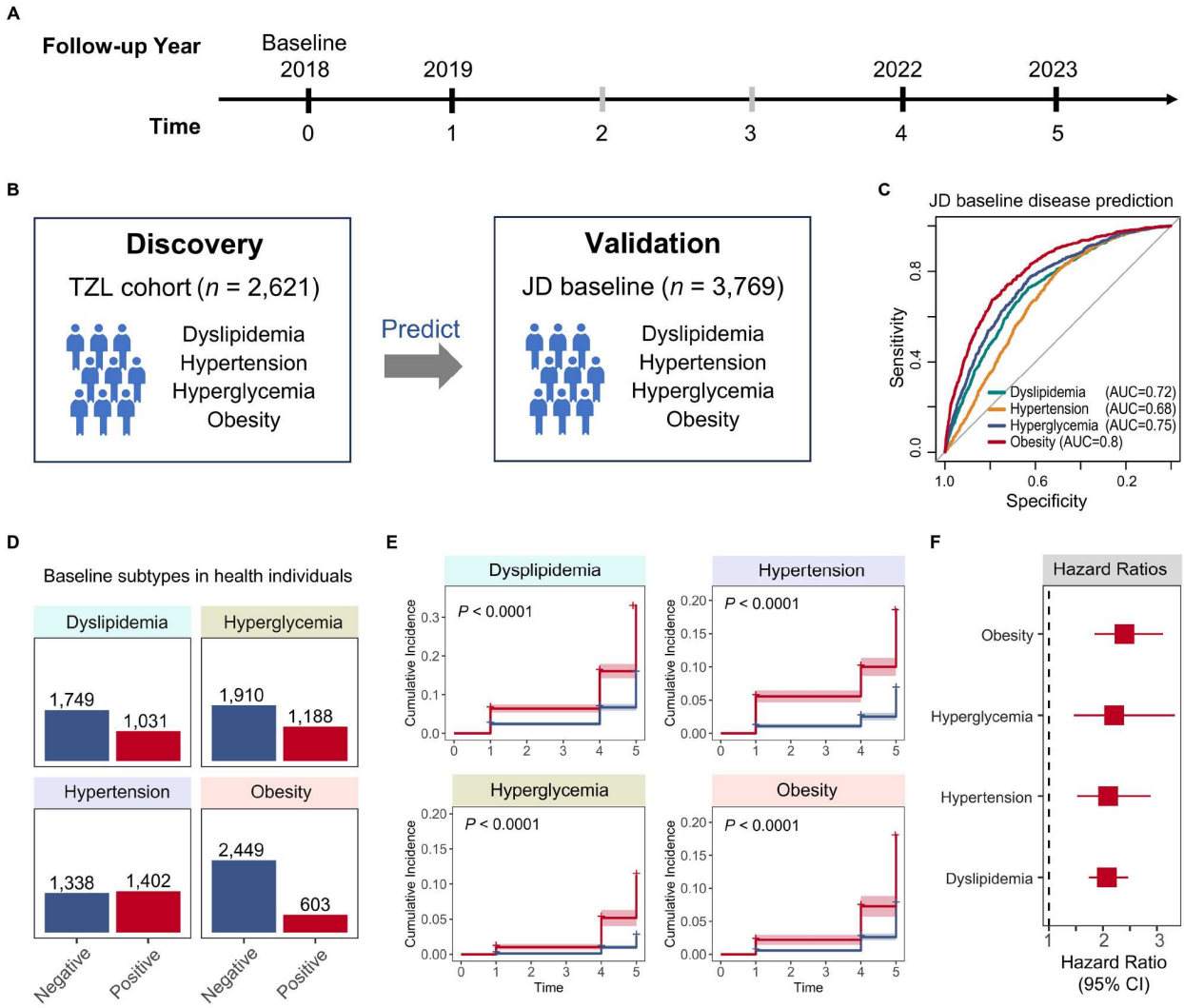

Figure 8. Longitudinal Data Validation of Future Disease Risk in Healthy Subtype. A, Longitudinal cohort baseline and follow-up sampling time points. B, The prediction models for the four diseases developed using the discovery cohort (TZL) were applied to the baseline data of the longitudinal validation set to obtain the predicted values for the corresponding diseases. C, ROC curves of the four diseases prediction performance at baseline in the longitudinal validation set. D, The predicted subgroups in baseline healthy individuals (negatives and positives). Negatives: Healthy individuals correctly predicted to remain disease-free. Positives: Healthy individuals predicted as diseased. E, Five-year cumulative incidence curves for the four metabolic diseases in the health subgroups. The curves are likely color-coded: Red: Represents the predicted positives, showing the proportion who develop the disease within five years. Blue: Represents the predicted negatives, showing the proportion who develop disease within five years. F, Hazard ratios for the four diseases over the next five years. Hazard ratios indicate the relative risk of developing a disease in the predicted positive group compared to the predicted negative group.

we categorized individuals within the healthy population into two subgroups: predicted negative and predicted positive (Figure 8D). For instance, among the 3,052 individuals with normal BMI at baseline, 2,449 were correctly predicted as having normal BMI (negative), and 603 were predicted as overweight (positive). Similarly, among the 3,098 individuals without hyperglycemia at baseline, 1,910 were correctly predicted as negative, and 1,188 were predicted as positive (Figure 8D).

To assess if the baseline predicted subgroup influences the likelihood of developing a disease in the future, we employed the Cox proportional hazards model, considering both follow-up time and disease status. The future disease incidence curves indicate that the disease development rate (incidence) over time within the baseline predicted positive group is significantly higher than that within the negative group (Figure 8E). The hazard ratios (HR) also confirm this, showing that for each disease, the baseline subgroup predicted as positive has a significantly higher risk of developing the disease compared to the subgroup predicted as negative. For example, the subgroup predicted as positive in the baseline normal BMI samples had a 2.40-fold higher risk of developing obesity (Hazard ratio=2.40, 95% CI: 1.84–3.12) over the next 5 years than the subgroup predicted as negative (Figure 8F). Likewise, the subgroup predicted as positive in the baseline normoglycemic samples had a 2.21-fold higher risk of developing hyperglycemia (Hazard ration=2.21, 95% CI: 1.46–3.33) over the next 5 years than the subgroup predicted as negative (Figure 8F).

DISCUSSION

The main goal of this study is to explore the potential application of facial features in predicting health. First, we employed a

https://doi.org/10.1007/s11427-024-2726-8

comprehensive facial analysis technique (FaWAS) to reveal a significant association between facial characteristics and MetS, along with related metabolic issues. Nearly half of the facial features we examined were linked to MetS risk, confirmed by follow-up studies and holding true for both men and women. This finding extends to other MetS-related conditions, highlighting the potential of facial features as predictive markers. Second, we delved deeper to understand the reasons behind this link, analyzing both genetic and environmental factors. Interestingly, our findings suggest that genetics play a more significant role in the association between facial features and metabolic health. Third, by creating models based on facial characteristics, we demonstrated the feasibility of using facial analysis for early detection and classification of MetS and other metabolic disorders. This opens doors for potential future applications in healthcare. Fourth, this research goes beyond just predicting health risks. We delved into the clinical implications of facial feature-based health prediction and defined health subtypes based on facial characteristics. This innovative approach is groundbreaking in this field. Similar to a study using multi-omics data to classify obesity subtypes, we found that facial feature-based prediction of health subtypes also holds clinical value. Finally, we introduced a longitudinal study to validate the potential of facial feature-defined health subtypes in identifying individuals at high risk of developing certain diseases. This research paves the way for a novel approach to assess metabolic health and potentially predict risks based on facial features. Further research is needed to refine and validate this approach for wider use.

Previous studies utilizing 2D imaging have identified key facial features associated with higher BMI, such as broader and shorter lower jaws, wider upper faces, and a noticeable distance between the eyebrows and eyes. These characteristics have been quantified using ratios like CJWR, WHR, LF/FH, and PAR, as well as measures like FW/LFH and MEH (Figure S4) (Stephen et al., 2017; Wen and Guo, 2013). Our study, employing 3D facial imaging, not only corroborates these 2D findings but also enriches our understanding by revealing that the increased distance between the eyebrows and eyes involves not just a vertical stretch but also an outward projection, enhancing the fullness of the temple-eye-cheek region in a 3D context. This shift to 3D imaging represents a significant improvement in the accuracy and depth of obesity prediction. While 2D imaging-based obesity predictions previously did not surpass an AUC of 0.80 (Fook et al., 2020; Raj et al., 2023; Wen and Guo, 2013; Yousaf et al., 2021), our 3D model excels with an AUC of 0.89. This noticeable improvement underscores the superiority of 3D imaging in capturing the complex facial features associated with obesity, offering a promising avenue for future non-invasive health assessments. By leveraging the comprehensive spatial data provided by 3D technology, we significantly enhance the precision of predicting health risks, paving the way for improved early detection and management strategies for MetS risk and related conditions.

Our study highlights the advantage of using 3D facial data in predicting disease, particularly in identifying subtypes within both healthy and diseased populations. The capability of our face-inferred model to detect nuanced subtypes across conditions like hypertension, hyperglycemia, lipid abnormalities, and obesity, underscores the potential of facial phenotyping in capturing the heterogeneity of health statuses. In addition, this study also includes a longitudinal cohort data and shows that the future 5-year risk of disease in the health subtype is significantly higher than the other subgroup. This suggests that facial features hold significant value in predicting future health problems, particularly metabolic issues. This finding aligns with omics-based predictions known for their biological relevance in identifying health subtypes (Watanabe et al., 2023). However, our study opens new questions about the unique contributions of facial phenotyping to this area. Future research should explore the synergistic potential of combining facial and omics data to enhance subtype distinction, offering deeper insights and improved strategies for understanding and managing health variations within populations.

The face-inferred model emerges as a highly accessible tool for self-health monitoring, distinguishing itself from other non-invasive measurement techniques (Hanna et al., 2020; Lee et al., 2019; Park et al., 2020) by leveraging solely 3D facial images for input. This approach not only demonstrates scalability for expanding datasets but also offers the groundwork for developing into user-friendly, portable software applications. Crucially, our methodology underscores a commitment to personal privacy protection. By employing the MeshMonk method (White et al., 2019) for the extraction of facial points and utilizing PCA for the compression of facial features, we ensure that personal identifiers are meticulously obscured, safeguarding sensitive information. This integration of privacy-preserving technologies with the face-inferred model enhances its appeal for widespread use, promising a seamless and secure avenue for individuals to monitor their health status. The potential for this model to be developed further into an intuitive, portable application underscores its future role in facilitating proactive health management and fostering a deeper understanding of personal health trends and predispositions.

Our study faces certain limitations, including incomplete disease information, which restricts the full exploration of 3D facial data's predictive capabilities for various diseases, suggesting the need for comprehensive clinical datasets in future research. Additionally, our model's reliance on PCA and linear regression may limit its effectiveness; future research could explore the potential of advanced deep learning techniques for improved outcomes. While our longitudinal study demonstrates the clinical significance of facial phenotype prediction in identifying subhealth or disease subtypes in metabolic diseases, our predictive model is currently based on cross-sectional data. This means it can only establish a correlation and interpretability between facial features and metabolic diseases. However, the underlying mechanisms by which predicted subtypes may have different future disease risks remain unclear and require further investigation. Additionally, although this study provides initial insights into the genetic and environmental factors contributing to the observed association between metabolic diseases and facial phenotypes, a more comprehensive phenome and exposome approach is necessary to fully understand the relationship between environmental factors and phenotypes. Lastly, our findings, derived from an East Asian cohort, highlight the necessity of extending this research to diverse populations to assess the model's universal applicability and ensure its generalizability across different demographic groups.

In conclusion, our study demonstrates the promising potential of using 3D facial imaging for predicting metabolic syndrome and related conditions, revealing significant associations between

facial features and health statuses. Despite facing limitations such as incomplete disease data and a focus on specific analytical models and populations, this research opens new avenues for non-invasive health monitoring and personalized medicine. The face-inferred model's scalability, privacy protection, and the novel insights it provides into disease subtyping underscore its value as a tool for future health assessment and management. As we move forward, expanding the dataset diversity and employing advanced analytical techniques will be crucial in enhancing the model's predictive accuracy and applicability across broader populations, marking a step forward in integrating facial phenotyping into health care practices.

MATERIALS AND METHODS

Study cohorts

Our study includes two distinct cohorts for discovery and validation purposes. The discovery cohort is drawn from the Taizhou Longitudinal Study (TZL) (Wang et al., 2009) and comprises 2,621 Chinese individuals, all of whom were volunteers recruited in Taizhou, Jiangsu Province, China. This group consists of 1,334 women and 786 men, ranging in age from 31 to 85 years and 34 to 88 years, respectively. The TZL study received approval from the Ethics Committee of Fudan University, Shanghai, China, and all participants in this cohort have given their written informed consent.

The validation cohort, on the other hand, includes 2,188 individuals from the National Survey of Physical Traits (NSPT) (Peng et al., 2024). The participants in this cohort were volunteers recruited in three Chinese provinces: Jiangsu, Henan, and Guangxi. This group comprises 1,356 women and 778 men, aged between 19 and 80 years for women and 19 and 83 years for men. Like the TZL, the NSPT also received ethical clearance from the Ethics Committee of Fudan University, Shanghai, China, and all individuals in this cohort have provided their written informed consents.

The longitudinal cohort, Jidong cohort (JD), includes 3,769 individuals who had 3D facial scans taken at baseline (year 2018) (Xia et al., 2020). Additionally, the cohort has clinical information related to four metabolic diseases (obesity, hypertension, hyperglycemia, and dyslipidemia) collected in 2018 (baseline), 2019, 2022, and 2023. This study was carried out according to the guidelines of the Declaration of Helsinki. Approval was obtained from Ethical Committees of the Staff Hospital of Jidong oil-field of China National Petroleum Corporation. The approval will be renewed every 5 years. Written informed consent was obtained from each of the participants.

3D facial image acquisition and processing

Our methodology for 3D facial image collection involved several steps to ensure accuracy and consistency. Initially, volunteers were asked to remove any makeup, glasses, or other items that could alter the appearance of their neutral face. They were also instructed to adopt a standard posture by sitting upright, facing directly forward, and pulling back their hair to reveal the forehead. Following image capture, each 3D image underwent manual inspection to exclude low-quality images or those showing facial expressions. This process was prior to the automated image alignment, during which individual texture information was disregarded.

The images were captured using a high-resolution 3D camera system (3dMD face system, www.3dmd.com/3dMDface). We then applied dense non-rigid registration to align the 3D images based on anatomical homology (Guo et al., 2013). The images were imported into MeshMonk software in wavefront .obj format for dense surface registration (White et al., 2019).

For initial alignment in MeshMonk, the nose tip landmark was manually identified as the origin point in each image, standardizing to 7,906 facial landmarks across all images. We conducted Generalized Procrustes Analysis (GPA) separately in TZL and NSPT groups to neutralize variations in position, orientation, and scale. Non-symmetric variations were averaged out. Each image and its landmarks underwent a thorough double-check to remove any prominent outliers.

Finally, after quality control (QC) procedures, the aligned images were projected into a 3D Euclidean space, considering the nose tip as the origin (x=0, y=0, z=0). We used the x, y, and z coordinates of all 7,906 landmarks as explanatory variables in subsequent association and prediction analysis, resulting in a total of 23,718 explanatory variables. Width is represented by the x-axis, with positive values extending to the right. Length is depicted on the y-axis, with positive values going upwards towards the top of the head. Finally, convexity is shown on the z-axis, with positive values indicating outward protrusion. We leverage this coordinate system to describe the relationship between facial characteristics and metabolic conditions.

Phenotyping

Anthropometric measurements

All anthropometrics and blood pressure were measured by physicians in Taizhou Institute of Health Sciences, Fudan University, who had been well trained by the research team. Weight was measured on a digital scale while subjects wore light clothing with no shoes. Height was determined using a wall-mounted measuring tape, subjects standing with no shoes. BMI is calculated by dividing weight in kilograms (kg) by the square of height in meters (m^2). Waist circumference (WC) was measured in standing subjects using a flexible tape, midway between the lowest rib and the iliac crest.

Peripheral artery blood pressure measurement

Peripheral blood pressure was measured with a standard mercury sphygmomanometer, using the first and fifth Korotkoff sounds as the systolic and diastolic blood pressure, while the subjects were in a sedentary position, having rested for at least 5 minutes. The appropriate size cuff was determined based on arm circumference. The systolic blood pressure (SBP, measured in mmHg) and diastolic blood pressure (DBP, measured in mmHg) were measured three times, and the average of these three measurements was considered as the final measurement value.

Laboratory analyses

Blood samples were collected between 7 am and 10 am, after subjects had fasted for at least 12 hours. Blood samples were stored at 4°C, and delivered to the central laboratory in the Taizhou Institute of Health Sciences, Fudan University on the same day. Serum fasting blood glucose (GLU, mmol L^{-1}), high density lipoprotein cholesterol (HDL, mmol L^{-1}), and low density

https://doi.org/10.1007/s11427-024-2726-8

lipoprotein cholesterol (LDL, mmol L^{-1}), total cholesterol (CH, mmol L^{-1}) and triglyceride (TG, mmol L^{-1}) levels were determined using enzymatic assays (Roche, Basel, Switzerland), on a fully automatic biochemical autoanalyzer (Cobas® 6000, Roche). The technicians who performed the different tests were blinded to the clinical data of the subjects.

Diseases

In our study, the definition of MetS adheres to the criteria of the revised ATP III. An individual is classified as having MetS if they exhibit three or more of the following conditions: (i) Central obesity, defined as a waist circumference (WC) of ⩾90 cm for men and ⩾80 cm for women; (ii) Elevated triglycerides (TG) level of ⩾1.7 mmol L^{-1} or undergoing treatment for high triglycerides; (iii) Redu ced High-Density Lipoprotein (HDL) cholesterol, indicated by levels <40 mg/dL (1.03 mmol L^{-1}) in men and <50 mg dL^{-1} (1.3 mmol L^{-1}) in women, or receiving treatment for low HDL; (iv) High blood pressure, characterized by systolic blood pressure (SBP) ⩾130 mmHg or diastolic blood pressure (DBP) ⩾85 mmHg, or treatment for previously diagnosed hypertension; (v) Elevated fasting plasma glucose (GLU) of ⩾5.6 mmol L^{-1}, or treatment for high glucose levels. Obesity is defined as a Body Mass Index (BMI) of ⩾28 kg m^{-2}. Dyslipidemia is identified by one or more of the following: Total Cholesterol (CH) ⩾6.22 mmol L^{-1}, Low-Density Lipoprotein (LDL) cholesterol ⩾4.14 mmol L^{-1}, HDL cholesterol <1.04 mmol L^{-1}, TG ⩾2.26 mmol L^{-1}, or a self-reported history of hyperlipidemia. Hypertension is defined either by a self-reported history of the condition or by having an SBP ⩾140 mmHg and/or a DBP ⩾90 mmHg. Hyperglycemia follows the current American Diabetes Association (ADA) criteria, defined as a fasting plasma glucose level of ⩾7.0 mmol L^{-1} or a self-reported history of diabetes.

Several exposed factors were extracted from the questionnaire, including living environment (rural or urban), smoking status (smoking or not), alcohol consumption (drinking or not), income and education status.

FaWAS

GWAS has proven to be a powerful tool in advancing our understanding of the genetic basis of various complex traits. Like GWAS, which iteratively tests the association between genome-wide genetic factors and the targeted phenotype, our FaWAS iteratively tests all facial traits with each binary phenotype, i.e., MetS, Obesity, Dyslipidemia, Hypertension, and Hyperglycemia, using logistic regression. For quantitative phenotypes such as BMI and SBP, we used linear regression. All association tests were adjusted for age and sex. Bonferroni method was used to derive our face-wide significant threshold ($P=2.11\times10^{-6}$). Replication was conducted using the same logistic or linear models where the resultant P values were Bonferroni adjusted. Sex stratified association analyses were conducted separately for males and females using the same logistic or linear models.

Prediction analysis

In our predictive analysis, we initially performed PCA on 23,718 facial variables, extracting 50 PCs that collectively accounted for 90% of the variance in facial features. Subsequently, we identified significant PCs associated with the disease status (sigPCs) and integrated them into the predictive model. The model, a multiple linear or logistic regression, included age and sex as covariates. Thorough evaluation of these models took place in TZL through a 10-fold cross-validation design.

In the 10-fold cross-validation procedure, the TZL dataset was randomly partitioned into ten subsets. In each fold, nine subsets served as the training set, while the remaining one functioned as the testing set. Feature selection was restricted to the training set in each fold, meaning that only significant PCs were employed to build the predictive models. To address overfitting, PCA was exclusively performed within the training set for each fold. Subsequently, the selected PCs in the testing set were predicted using the PCA model from the training set, eliminating the necessity for PCA in the testing set.

The performance of models trained on all TZL samples was externally validated using the NSPT dataset. For continuous outcomes, model predictive performance was assessed using the coefficient of determination (R^2) and Mean Absolute Error (MAE). For binary outcomes, we evaluated the models using statistical metrics including the Area Under the Receiver Operating Characteristic Curve (AUC), sensitivity, specificity, and the F1 score.

Multitask-based prediction for multiple diseases

The process begins with data preprocessing, where categorical variables are converted to numeric, incomplete cases are removed, and labels are converted to logical. Next, a multi-label task is defined with the target labels. In this step, two multitask-based prediction methods were applied. One is based on R randomForest package. The model definition involves choosing a base learner, specifically a random forest, and wrapping it for multi-label classification. The multi-label model is then trained on the preprocessed data. Finally, the trained model is used to predict labels for an external data (NSPT). For another one, a multivariate regression model is trained using the rfsrc function from the R randomForestSRC package, which handles multiple regression targets simultaneously. These approaches allow for simultaneous modeling and prediction of multiple related outcomes, leveraging shared information among the labels for potentially improved predictive performance.

For comparison, we also applied a single-task-based prediction model based on R randomForestSRC package. This method involves building and using multiple regression models for predicting several disease-related labels. First, categorical variables in both training and testing datasets are converted to numeric, and incomplete cases are removed to ensure clean data. The specified disease labels are ensured to be numeric. For each label, a regression task is created, and a random forest regression learner is defined and trained on the corresponding data. Predictions are then made for the external datasets using the respective models.

Analyzing future disease risk with cox proportional hazards model

To assess the risk of developing different diseases in our longitudinal data, we employed the Cox proportional hazards model (implemented with coxph from survival). This model estimates how factors like age, sex, and group (explanatory variables) influence the likelihood of developing a disease

(survival outcome) defined by follow-up time and disease status. The model provides hazard ratios (HR) and their confidence intervals (CI). To effectively communicate these risk estimates, we generated a forest plot using the ggplot2 library. This plot visually represents the HRs and their CIs for different disease categories, allowing for easy comparison of risk factors across various diseases. Furthermore, we utilized survfit from the survival package to estimate future disease incidence curves. These curves depict the disease development rate (incidence) over time within different groups. The visualization of these cumulative incidence curves is generated using ggsurvplot from the survminer package.

Heritability and genetic correlation

The microarray data and quality control (QC) procedures in TZL and NSPT have been comprehensively detailed in a previous publication (Zhang et al., 2022). In essence, TZL and NSPT utilized distinct gene typing platforms: the Illumina Infinium Global Screening Array, designed by WeGene (https://www.wegene.com/), capturing 707,180 variants, and the Illumina HumanOmniZhongHua-8 array, capturing 776,213 variants, respectively. Quality control and imputation were independently conducted for each dataset. Following the completion of all QC steps (Minor Allele Frequency>0.05, Hardy-Weinberg Equilibrium P-value>10^{-5}, INFO score>0.8), a total of 8,018,212 shared variants between the discovery and replication datasets were obtained for subsequent analysis. Unsupervised k-means clustering of the three main genomic PCs demonstrated that our samples are closely grouped with East Asians from the 1000 Genomes Project. GCTA (https://cnsgenomics.com/software/gcta/) (Yang et al., 2011; Yang et al., 2016) was employed to estimate SNP-based heritability for facial PCs and MetS and to evaluate genetic correlations between facial PCs and MetS.

All statistical analyses were conducted in R 4.2.2 unless otherwise specified.

Compliance and ethics

The authors declare that they have no conflict of interest. The discovery and validation datasets (TZL and NSPT) received approval from the Ethics Committee of Fudan University, Shanghai, China (No. 14117). All procedures performed in the study involving human participants were in accordance with the ethical standards of the institutional and/or national research committee and with the Declaration of Helsinki and its later amendments or comparable ethical standards.

Acknowledgement

This work was supported by the National Key R&D Program of China (2024YFC3405800 to S.W.), the Strategic Priority Research Program of the Chinese Academy of Sciences (XDB38020400 to S.W.), CAS Youth Innovation Promotion Association (2020276 to Q.P.), CAS Young Team Program for Stable Support of Basic Research (YSBR-077 to S.W.), CAS Interdisciplinary Innovation Team to S.W., Shanghai Municipal Science and Technology Major Project (2017SHZDZX01 to S.W., L.J., J.W., J.T., and Q.P.), Shanghai Science and Technology Innovation Action Project (24JS2810300 to S.W.), the National Natural Science Foundation of China (32325013, 92249302 to S.W., 32471216 to Q.P., 32271186 to J.T.), the National Key Research and Development Project (2018YFC0910403 to S.W.), Ministry of Science and Technology of the People's Republic of China (2015FY111700 to L.J.), Shanghai Science and Technology Commission Excellent Academic Leaders Program (22XD1424700 to S.W.), 111 Project (B13016 to L.J.), and CAMS Innovation Fund for Medical Science (2019-I2M-5-066 to J.W. and L.J.).

Supporting information

The supporting information is available online at https://doi.org/10.1007/s11427-024-2726-8. The supporting materials are published as submitted, without typesetting or editing. The responsibility for scientific accuracy and content remains entirely with the authors.

References

Agirbasli, M., and Aksoy, A. (2019). Letter by Agirbasli and Aksoy regarding article, "Associations of variability in blood pressure, glucose and cholesterol concentrations, and body mass index with mortality and cardiovascular outcomes in the general population". Circulation 139, e911.

Bhuiyan, Z.A., Klein, M., Hammond, P., van Haeringen, A., Mannens, M.M.A.M., Van Berckelaer-Onnes, I., and Hennekam, R.C.M. (2006). Genotype-phenotype correlations of 39 patients with Cornelia De Lange syndrome: the Dutch experience. J Med Genet, 43: 568-575..

Bonfante, B., Faux, P., Navarro, N., Mendoza-Revilla, J., Dubied, M., Montillot, C., Wentworth, E., Poloni, L., Varón-González, C., Jones, P., et al. (2021). A GWAS in Latin Americans identifies novel face shape loci, implicating VPS13B and a Denisovan introgressed region in facial variation. Sci Adv 7, eabc6160.

Cai, X., Hu, D., Pan, C., Li, G., Lu, J., Ji, Q., Su, B., Tian, H., Qu, S., Weng, J., et al. (2019). The risk factors of glycemic control, blood pressure control, lipid control in Chinese patients with newly diagnosed type 2 diabetes _ A nationwide prospective cohort study. Sci Rep 9, 7709.

Chen, K., Shen, Z., Gu, W., Lyu, Z., Qi, X., Mu, Y., and Ning, Y. (2023). Prevalence of obesity and associated complications in China: A cross-sectional, real-world study in 15.8 million adults. Diabetes Obesity Metab 25, 3390–3399.

Cox-Brinkman, J., Vedder, A., Hollak, C., Richfield, L., Mehta, A., Orteu, K., Wijburg, F., and Hammond, P. (2007). Three-dimensional face shape in Fabry disease. Eur J Hum Genet 15, 535–542.

Cui, Y., and Leclercq, S. (2017). Environment-related variation in the human Mid-Face. Anatomical Record 300, 238–250.

Doosti-Irani, A., Mansournia, M.A., and Collins, G. (2019). Letter by Doosti-Irani et al regarding article, "Associations of variability in blood pressure, glucose and cholesterol concentrations, and body mass index with mortality and cardiovascular outcomes in the general population". Circulation 139, e909.

Fook, C.Y., Chin, L.C., Vijean, V., Teen, L.W., Ali, H., and Nasir, A.S.A. (2020). Investigation on body mass index prediction from face images. In 2020 IEEE-EMBS Conference on Biomedical Engineering and Sciences (IECBES), Langkawi Island, Malaysia, 2021, pp. 543-548..

Ge, H., Yang, Z., Li, X., Liu, D., Li, Y., Pan, Y., Luo, D., and Wu, X. (2020). The prevalence and associated factors of metabolic syndrome in Chinese aging population. Sci Rep 10, 20034.

Grundy, S.M., Cleeman, J.I., Daniels, S.R., Donato, K.A., Eckel, R.H., Franklin, B.A., Gordon, D.J., Krauss, R.M., Savage, P.J., Smith Jr, S.C., et al. (2005). Diagnosis and management of the metabolic syndrome. Circulation 112, 2735–2752.

Gunn, D.A., Dick, J.L., van Heemst, D., Griffiths, C.E.M., Tomlin, C.C., Murray, P.G., Griffiths, T.W., Ogden, S., Mayes, A.E., Westendorp, R.G.J., et al. (2015). Lifestyle and youthful looks. Br J Dermatol 172, 1338–1345.

Guo, J., Mei, X., and Tang, K. (2013). Automatic landmark annotation and dense correspondence registration for 3D human facial images. BMC BioInf 14, 232.

Gurovich, Y., Hanani, Y., Bar, O., Nadav, G., Fleischer, N., Gelbman, D., Basel-Salmon, L., Krawitz, P.M., Kamphausen, S.B., Zenker, M., et al. (2019). Identifying facial phenotypes of genetic disorders using deep learning. Nat Med 25, 60–64.

Hammond, P. (2007). The use of 3D face shape modelling in dysmorphology. Arch Dis Child, 92: 1120-1126..

Hammond, P., Forster-Gibson, C., Chudley, A.E., Allanson, J.E., Hutton, T.J., Farrell, S. A., McKenzie, J., Holden, J.J.A., and Lewis, M.E.S. (2008). Face–brain asymmetry in autism spectrum disorders. Mol Psychiatry 13, 614–623.

Hammond, P., Hutton, T.J., Allanson, J.E., Buxton, B., Campbell, L.E., Clayton-Smith, J., Donnai, D., Karmiloff-Smith, A., Metcalfe, K., Murphy, K.C., et al. (2005). Discriminating power of localized three-dimensional facial morphology. Am J Hum Genet 77, 999–1010.

Hammond, P., Hutton, T.J., Allanson, J.E., Campbell, L.E., Hennekam, R.C.M., Holden, S., Patton, M.A., Shaw, A., Temple, I.K., Trotter, M., et al. (2004). 3D analysis of facial morphology. Am J Med Genet Pt A 126A, 339–348.

Hanna, J., Bteich, M., Tawk, Y., Ramadan, A.H., Dia, B., Asadallah, F.A., Eid, A., Kanj, R., Costantine, J., and Eid, A.A. (2020). Noninvasive, wearable, and tunable electromagnetic multisensing system for continuous glucose monitoring, mimicking vasculature anatomy. Sci Adv 6, eaba5320.

Hong, K.N., Fuster, V., Rosenson, R.S., Rosendorff, C., and Bhatt, D.L. (2017). How low to go with glucose, cholesterol, and blood pressure in primary prevention of CVD. J Am Coll Cardiol 70, 2171–2185.

Huang, Y., Chen, Z., Wang, X., Zheng, C., Shao, L., Tian, Y., Cao, X., Tian, Y., Gao, R., Zhang, L., et al. (2023). Comparison of the three most commonly used metabolic syndrome definitions in the Chinese population: a prospective study. Metabolites 13, 12.

Khunti, K., Kosiborod, M., and Ray, K.K. (2018). Legacy benefits of blood glucose, blood pressure and lipid control in individuals with diabetes and cardiovascular disease: Time to overcome multifactorial therapeutic inertia? Diabetes Obesity Metab 20, 1337–1341.

Kim, M.K., Han, K., Park, Y.M., Kwon, H.S., Kang, G., Yoon, K.H., and Lee, S.H. (2018). Associations of variability in blood pressure, glucose and cholesterol

concentrations, and body mass index with mortality and cardiovascular outcomes in the general population. Circulation 138, 2627–2637.
Kontopantelis, E., Springate, D.A., Reeves, D., Ashcroft, D.M., Rutter, M., Buchan, I., and Doran, T. (2015). Glucose, blood pressure and cholesterol levels and their relationships to clinical outcomes in type 2 diabetes: A retrospective cohort study. Diabetologia 58, 505–518.
Lee, S.H., Cho, Y.C., and Bin Choy, Y. (2019). Noninvasive self-diagnostic device for tear collection and glucose measurement. Sci Rep 9, 4747.
Li, Y., Teng, D., Shi, X., Qin, G., Qin, Y., Quan, H., Shi, B., Sun, H., Ba, J., Chen, B., et al. (2020). Prevalence of diabetes recorded in the mainland of China using 2018 diagnostic criteria from the American Diabetes Association: National cross sectional study. BMJ 369, m997.
Liu, M., and Feng, J. (2023). Association between adiposity and facial aging: Results from a Mendelian randomization study. Eur J Med Res 28, 350.
Liu, Z., Mi, J., and Wu, H. (2023). Relationships between circulating metabolites and facial skin aging: A Mendelian randomization study. Hum Genomics 17, 23.
Lu, Y., Zhang, H., Lu, J., Ding, Q., Li, X., Wang, X., Sun, D., Tan, L., Mu, L., Liu, J., et al. (2021). Prevalence of dyslipidemia and availability of lipid-Lowering medications among primary health care settings in China. JAMA Netw Open 4, e2127573.
Mu, L., Liu, J., Zhou, G., Wu, C., Chen, B., Lu, Y., Lu, J., Yan, X., Zhu, Z., Nasir, K., et al. (2021). Obesity prevalence and risks among Chinese adults: findings from the China PEACE million persons project, 2014–2018. Circ-Cardiovasc Qual Outcomes 14, e007292.
Musani, S.K., Martin, L.J., Woo, J.G., Olivier, M., Gurka, M.J., and DeBoer, M.D. (2017). Heritability of the Severity of the Metabolic Syndrome in Whites and Blacks in 3 Large Cohorts. Circ Cardiovasc Genet 10, e001621.
Park, E.Y., Baik, J., Kim, H., Park, S.M., and Kim, C. (2020). Ultrasound-modulated optical glucose sensing using a 1645 nm laser. Sci Rep 10, 13361.
Peng, Q., Liu, X., Li, W., Jing, H., Li, J., Gao, X., Luo, Q., Breeze, C.E., Pan, S., Zheng, Q., et al. (2024). Analysis of blood methylation quantitative trait loci in East Asians reveals ancestry-specific impacts on complex traits. Nat Genet 56, 846–860.
Peng, Q., Liu, Y., Huels, A., Zhang, C., Yu, Y., Qiu, W., Cai, X., Zhao, Y., Schikowski, T., Merches, K., et al. (2023). Genetic variants in telomerase reverse transcriptase contribute to solar lentigines. J Investig Dermatol 143, 1062–1072.e25.
Raj, V.D., Motkar, S., Swamy, N.Y., Sanjana, N., and Sultana, S. (2023). Prediction of BMI from facial image using deep learning. International Research Journal of Engineering and Technology (IRJET) 10, 671–674..
Rana, S., Ali, S., Wani, H.A., Mushtaq, Q.D., Sharma, S., and Rehman, M.U. (2022). Metabolic syndrome and underlying genetic determinants-A systematic review. J Diabetes Metab Disord 21, 1095–1104.
Rippe, J.M. (2018). Lifestyle medicine: the health promoting power of daily habits and practices. Am J Lifestyle Med 12, 499–512.
Rutter, M.K., and Nesto, R.W. (2011). Blood pressure, lipids and glucose in type 2 diabetes: How low should we go? Re-discovering personalized care. Eur Heart J 32, 2247–2255.
Saklayen, M.G. (2018). The global epidemic of the metabolic syndrome. Curr Hypertens Rep 20, 12.
Santos, L. (2022). The impact of nutrition and lifestyle modification on health. Eur J Internal Med 97, 18–25.
Stephen, I.D., Hiew, V., Coetzee, V., Tiddeman, B.P., and Perrett, D.I. (2017). Facial shape analysis identifies valid cues to aspects of physiological health in Caucasian, Asian, and african populations. Front Psychol 8, 1883.
Tobin, J.L., Di Franco, M., Eichers, E., May-Simera, H., Garcia, M., Yan, J., Quinlan, R., Justice, M.J., Hennekam, R.C., Briscoe, J., et al. (2008). Inhibition of neural crest migration underlies craniofacial dysmorphology and Hirschsprung's disease in Bardet–Biedl syndrome. Proc Natl Acad Sci USA 105, 6714–6719.
Tsigos, C., Bitzur, R., Kleinman, Y., Cohen, H., Cahn, A., Brambilla, G., Mancia, G., and Grassi, G. (2013). Targets for body fat, blood pressure, lipids, and glucose-lowering interventions in healthy older people. Diabetes Care 36, S292–S300.
Wang, X., Lu, M., Qian, J., Yang, Y., Li, S., Lu, D., Yu, S., Meng, W., Ye, W., and Jin, L. (2009). Rationales, design and recruitment of the Taizhou Longitudinal Study. BMC Public Health 9, 223.
Watanabe, K., Wilmanski, T., Diener, C., Earls, J.C., Zimmer, A., Lincoln, B., Hadlock, J.J., Lovejoy, J.C., Gibbons, S.M., Magis, A.T., et al. (2023). Multiomic signatures of body mass index identify heterogeneous health phenotypes and responses to a lifestyle intervention. Nat Med 29, 996–1008.
Wen, L., and Guo, G. (2013). A computational approach to body mass index prediction from face images. Image Vis Comput 31, 392–400.
White, J.D., Indencleef, K., Naqvi, S., Eller, R.J., Hoskens, H., Roosenboom, J., Lee, M. K., Li, J., Mohammed, J., Richmond, S., et al. (2021). Insights into the genetic architecture of the human face. Nat Genet 53, 45–53.
White, J.D., Ortega-Castrillón, A., Matthews, H., Zaidi, A.A., Ekrami, O., Snyders, J., Fan, Y., Penington, T., Van Dongen, S., Shriver, M.D., et al. (2019). MeshMonk: Open-source large-scale intensive 3D phenotyping. Sci Rep 9, 6085.
Xia, X., Chen, X., Wu, G., Li, F., Wang, Y., Chen, Y., Chen, M., Wang, X., Chen, W., Xian, B., et al. (2020). Three-dimensional facial-image analysis to predict heterogeneity of the human ageing rate and the impact of lifestyle. Nat Metab 2, 946–957.
Xiong, Z., Dankova, G., Howe, L.J., Lee, M.K., Hysi, P.G., de Jong, M.A., Zhu, G., Adhikari, K., Li, D., Li, Y., et al. (2019). Novel genetic loci affecting facial shape variation in humans. eLife 8, e49898.
Xiong, Z., Gao, X., Chen, Y., Feng, Z., Pan, S., Lu, H., Uitterlinden, A.G., Nijsten, T., Ikram, A., Rivadeneira, F., et al. (2022). Combining genome-wide association studies highlight novel loci involved in human facial variation. Nat Commun 13, 7832.
Yang, J., Lee, S.H., Goddard, M.E., and Visscher, P.M. (2011). GCTA: a tool for genome-wide complex trait analysis. Am J Hum Genet 88, 76–82.
Yang, J., Lee, S.H., Wray, N.R., Goddard, M.E., and Visscher, P.M. (2016). GCTA-GREML accounts for linkage disequilibrium when estimating genetic variance from genome-wide SNPs. Proc Natl Acad Sci USA 113, E4579–E4580.
Yang, Y., Lyu, J., Wang, R., Wen, Q., Zhao, L., Chen, W., Bi, S., Meng, J., Mao, K., Xiao, Y., et al. (2022). A digital mask to safeguard patient privacy. Nat Med 28, 1883–1892.
Yin, R., Yin, L., Li, L., Silva-Nash, J., Tan, J., Pan, Z., Zeng, J., and Yan, L.L. (2022). Hypertension in China: Burdens, guidelines and policy responses: a state-of-the-art review. J Hum Hypertens 36, 126–134.
Yousaf, N., Hussein, S., and Sultani, W. (2021). Estimation of BMI from facial images using semantic segmentation based region-aware pooling. Comput Biol Med 133, 104392.
Zhang, M., Wu, S., Du, S., Qian, W., Chen, J., Qiao, L., Yang, Y., Tan, J., Yuan, Z., Peng, Q., et al. (2022). Genetic variants underlying differences in facial morphology in East Asian and European populations. Nat Genet 54, 403–411.
Zhao, X., Lu, C., Song, B., Chen, D., Teng, D., Shan, Z., and Teng, W. (2023). The prevalence and clustering of metabolic syndrome risk components in Chinese population: a cross-sectional study. Front Endocrinol (Lausanne) 14, 1290855.